

Numerical and asymptotic approaches to scattering problems involving finite elastic plates in structural acoustics

By Stefan G. Llewellyn Smith^a and Richard V. Craster^b

^aDepartment of Applied Mathematics and Theoretical Physics, University of Cambridge,
Silver Street, Cambridge, CB3 9EW, U.K.

^bDepartment of Mathematics, Imperial College of Science, Technology and Medicine, London,
SW7 2BZ, U.K.

(Received 7 September 1998)

An efficient, flexible and accurate numerical scheme for treating scattering problems involving clamped finite elastic plates is developed. Such problems are of particular interest in structural acoustics and have relevance to scattering by panels in underwater acoustics and aerodynamic noise. The scheme is applied to a single plate in a rigid baffle and also to a periodic array of elastic plates.

Considerable effort has been expended in the past to develop asymptotic methods for treating these problems in various limits such as ‘heavy’ or ‘light’ fluid loading or for wide strips. To validate the numerical scheme and also to demonstrate the ranges of validity of these approximations, comparisons between numerical and asymptotic solutions are made. The asymptotic methods are developed in some detail and some useful approximate formulae are identified.

1. Introduction

In structural acoustics vibrational energy is often carried by flexural plate waves which are only weakly coupled to the fluid in the absence of defects. It is only the presence of inhomogeneities and material discontinuities in the plate that allows significant radiation of energy into the fluid. Thus it is important to understand the mechanisms involved, as well as the relative influences of structural inertia, stiffness and fluid inertia, pressure and compressibility for specific model problems and ranges of material parameters. Considerable efforts have been spent over several decades analysing scattering by model defects; see for instance [1,2]. In various limits, the resulting solutions often demonstrate interesting and physically important effects, such as beam formation and resonance phenomena.

There are several problems that allow an exact solution. For instance scattering by isolated point defects, such as ribs, multiple ribs, cracked plates, and so on lead to exact solutions in terms of Fourier integrals; see for instance [3,4]. Another revealing class of problems is that concerned with joints between semi-infinite plates of differing material properties; these illustrate the importance of the edge conditions at the joint on the scattered field and the effect of the joint itself on the scattered field. A large variety of such problems, treated using the Wiener–Hopf technique, appears within the literature [5–7]. These model structural attachments, reinforcing ribs and baffled plates.

In reality of course, one is often interested in finite elastic plates and in the interaction

between the edges and perhaps also with other discontinuities that may be close to the edge. There are a variety of asymptotic approaches taking advantage of heavy or light fluid loading limits [8,9]. These isolate resonant phenomena in both heavy and light fluid loading limits and the beaming associated with leaky waves, amongst other effects. Similar approaches will be employed later in the text.

There are also numerical approaches using the modified Wiener–Hopf technique as in [10]; these are perhaps less flexible than the numerical method described later. In addition there are papers dealing with the situation when the plate is simply supported, that is, when $\eta = \eta' = 0$ at the plate edge (η is the plate displacement). In this case a simple modal expansion can be taken. However the simply supported case is arguably not the correct physical edge condition in many situations, as discussed by [11], and a more realistic situation is that of clamped edge conditions for which the simple modal method does not work. Analytical studies such as that of [5] show that the effect of the edge condition upon the scattered acoustic response is often significant, and thus it is important to model the edge behaviour accurately.

Our aim in this paper is to introduce and develop a fast, efficient, flexible and accurate numerical scheme to deal with finite elastic plate problems. To provide confidence in the numerical scheme, and to encourage further use in three-dimensional and other more complicated geometries, we validate the model in situations where one might expect errors to occur. That is, we concentrate upon providing asymptotic solutions near resonances. Other regimes where analytic inroads are possible, such as heavy and light fluid loading, are also investigated to show how the method performs. The method will work over a wide range of frequencies, for the clamped edge conditions, and also allows compliant loading effects to be analysed. It will be particularly useful in the regimes not amenable to asymptotic analyses and convenient for quite general incident fields. In general the scheme is also applicable to other geometries and boundary conditions [12], and to related problems, such as those incorporating fluid flow. In this paper we aim to verify the numerical scheme thoroughly against existing analytic work; this in turn highlights the range of applicability of the asymptotic methods, and some useful approximate solutions.

In view of the large amount of pre-existing analytic work, some of which has been mentioned above, we take maximal advantage of previous results by using integral equation and Green’s function approaches. There are some interesting facets to the resulting numerical approach, such as explicitly building in the correct edge behaviour, and reducing the kernel of the integral equation to a form suitable for rapid numerical evaluation. The approach is detailed for a finite elastic plate in a rigid baffle. The conditions at the joint between the baffle and plate will be taken to be clamped edge conditions, that is, both the plate displacement η and its gradient η' are zero across the joint. We then examine the approach in several differing limits which provides considerable confidence in its accuracy. To demonstrate the utility of this approach we also briefly consider a periodic array of elastic plates. In addition reciprocity and power balance results are also utilised as consistency checks on the numerics.

We consider time harmonic vibrations of frequency ω and all physical variables are assumed to have an $e^{-i\omega t}$ dependence. This is considered understood and is henceforth suppressed. Two dimensional problems are considered with an inviscid, compressible fluid lying in $x_3 > 0$ and $-\infty < x_1 < \infty$. The fluid pressure $p(x_1, x_3)$ satisfies

$$(\nabla^2 + k_0^2)p(x_1, x_3) = f(x_1, x_3), \quad (1.1)$$

where $f(x_1, x_3)$ corresponds to a distribution of fluid sources, and k_0 , the acoustic wavenumber, is related to the sound speed c_0 via $k_0 = \omega/c_0$. In what follows the source distribution is zero except for Green’s functions. The displacement in the x_3 -direction

within the fluid, $\eta(x_1, x_3)$, is related to the fluid pressure via

$$\rho\omega^2\eta(x_1, x_3) = \frac{\partial p(x_1, x_3)}{\partial x_3}. \quad (1.2)$$

The plane $x_3 = 0$ is taken in section 2 to consist of a thin elastic plate in the finite region $|x_1| < a$ and of a rigid plate elsewhere. When treating elastic plates the classical thin plate equation

$$B \frac{\partial^4 \eta(x_1, 0)}{\partial x_1^4} - m\omega^2 \eta(x_1, 0) = -p(x_1, 0) \quad (1.3)$$

is adopted [2]. The plate is assumed to separate fluid in the region $x_3 > 0$ from a vacuum in $x_3 < 0$. The geometry is depicted in figure 1. Apart from a membrane, this is the simplest model for a realistic wavebearing structure. Crucially it neglects transverse shear and rotary inertia effects, leading to a loss of accuracy for frequencies near to and above the coincidence frequency, at which the *in vacuo* and fluid wavespeeds are equal. Nonetheless the thin plate equation is widely used and often gives useful insights into the phenomena associated with scattering by elastic plates. Plane wave incidence, source irradiation and local excitation forcing can all be considered. The second case corresponds to a point source located in the fluid. In the last case, either a term $F_0\delta((x_1 - L)/a)$ or $G_0\delta'((x_1 - L)/a)$ is required on the right hand side of (1.3), corresponding to a line force or line moment respectively offset a distance L ($|L| < a$) from the centre of the plate.

The parameters B and m are the bending stiffness and mass per unit area of the plate respectively. Here we model mechanical attenuation by taking B to contain a small imaginary part and set $B = B_1 e^{-i\delta}$, with B_1 real. In practice viscoelastic materials may be used to dissipate energy carried by plate waves and thus reduce the radiated sound: [13] gives a typical value of δ as 0.2. These parameters are related to the properties of the elastic plate via $B_1 = Eh^3/12(1 - \nu^2)$ and $m = \rho_s h$, with E , h , ν , and ρ_s the Young's modulus, plate thickness, Poisson ratio and mass density of the elastic material respectively. In order to minimise the number of parameters that occur later, we introduce the *in vacuo* flexural wavenumber $k_p \equiv (\omega^2 m/B)^{1/4}$. Thus incorporating a small loss factor δ will lead to attenuation of the plate waves. Following [8] we introduce the non-dimensional quantities M and ϵ . The 'Mach' number M is defined to be the ratio of the fluid sound speed to that of the *in vacuo* plate waves, $M \equiv k_0/|k_p|$. A frequency-independent measure of fluid loading is provided by the parameter $\epsilon \equiv (B_1 \rho^2/m^3 c_0^2)^{1/2}$. For later convenience, we also define the complex quantity $\epsilon_c \equiv (B \rho^2/m^3 c_0^2)^{1/2} = e^{-i\delta/2} \epsilon$. In essence, when the system is lossless, there are three parameters that can be varied: M , ϵ and $k_0 a$, the last of these being the ratio of a typical lengthscale associated with the fluid disturbance to a typical lengthscale associated with the finite defect. Typically ϵ is small; for example $\epsilon \approx 0.134$ for steel plates in water, while M , which is frequency dependent, can range through all values. The fluid-loading will, as in [8], be termed 'light' when $M \sim O(1)$ but is not in the immediate neighbourhood of $M = 1$, and 'heavy' when $M \ll \epsilon$. In both cases ϵ is taken to be small, i.e. $\epsilon \ll 1$. To model coated plates the parameter δ may be varied.

In addition various edge conditions may be adopted at the end points of the elastic plates. In this paper we will take the clamped conditions $\eta(\pm a, 0) = \eta'(\pm a, 0) = 0$ to hold: these are the more relevant conditions for the attachment of a plate to a rigid baffle. However, other edge conditions such as a free joint ($\eta''(\pm a, 0) = \eta'''(\pm a, 0) = 0$) could be taken, which would alter some of the numerical aspects. The edge conditions in conjunction with the plate equations give the local behaviour of $\eta(x_1, 0)$ as $x_1 \rightarrow \pm a$. In the integral equation formulation adopted within the text the plate displacement,

Figure 1

$\eta(x_1, 0)$, is unknown along the finite region $|x_1| < a$. In related problems in elasticity and scalar wave diffraction, the local plate edge behaviour of the analogous functions is typically $O(a \pm x_1)^{\frac{1}{2}}$ or $O(a \pm x_1)^{-\frac{1}{2}}$ as $x_1 \rightarrow \mp a$. There are many examples of numerical approaches using Chebyshev polynomials or collocation methods in water waves and acoustics, for instance [14], and in elasticity, for instance [15,16]. A novel aspect of the elastic plate problems is that the edge conditions in the clamped case force the local behaviour to be $O(a^2 - x_1^2)^2$ as $x_1 \rightarrow \pm a$, which therefore requires a slightly different approach to be developed. It is envisaged that developing an accurate and fast numerical scheme will encourage further numerical studies in this area.

2. Formulation

The starting point is Green's theorem for two independent states $p(\mathbf{x})$ and $p^*(\mathbf{x})$ in a volume V bounded by a surface S :

$$\int_V [(\nabla^2 p + k_0^2 p)p^* - (\nabla^2 p^* + k_0^2 p^*)p] dV = \int_S (p^* p_{,i} - p p_{,i}^*) n_i dS, \quad (2.1)$$

where n_i is the outward-pointing normal to the surface. The starred field will be taken to be the Green's state

$$\nabla^2 p^G(\mathbf{x}; \mathbf{q}) + k_0^2 p^G(\mathbf{x}; \mathbf{q}) = -\delta(\mathbf{x} - \mathbf{q}), \quad (2.2)$$

where $\mathbf{x} = (x_1, x_3)$ is the variable in the gradient operator, and $\mathbf{q} = (q_1, q_3)$ is the position of the forcing function. A number of different conditions may be taken for $p^G(\mathbf{x}; \mathbf{q})$ or $\eta^G(\mathbf{x}; \mathbf{q})$ on $x_3 = 0$, depending on the precise problem. The unstarred field in (2.1) will be taken to be the scattered component of the total pressure. For the half-space $x_3 > 0$, Green's formula reduces to

$$p^{sc}(\mathbf{q}) = \rho\omega^2 \int_S [\eta^G(x_1, 0; \mathbf{q})p^{sc}(x_1, 0) - \eta^{sc}(x_1, 0)p^G(x_1, 0; \mathbf{q})] dx_1, \quad (2.3)$$

where S is simply the x_3 -axis. An integral equation for the displacement on the plate may be obtained by operating on (2.3) appropriately.

For the elastic plate set in a rigid baffle, we take the Green's state with $\eta^G(\mathbf{x}; \mathbf{q}) = 0$ on $x_3 = 0$. In this case, the appropriate Green's function is simply

$$p^G(\mathbf{x}; \mathbf{q}) = \frac{i}{4\pi} \int_C \frac{1}{\gamma_0} \left[e^{i\gamma_0|x_3 - q_3|} + e^{i\gamma_0(x_3 + q_3)} \right] e^{ik(x_1 - q_1)} dk, \quad (2.4)$$

which also has a representation in terms of Hankel functions. The function $\gamma_0 = (k_0^2 - k^2)^{\frac{1}{2}}$ has positive imaginary part (it is not yet necessary to specify its branch cuts beyond this; see however Appendix A). The boundary condition on $x_3 = 0$ for $|x_1| > a$ is $\eta(x_1, 0) = 0$, so the scattered pressure becomes

$$p^{sc}(\mathbf{q}) = -\rho\omega^2 \int_{-a}^a \eta^{sc}(x_1, 0)p^G(x_1, 0; \mathbf{q}) dx_1. \quad (2.5)$$

The plate displacement $\eta^{sc}(x_1, 0)$ is unknown in (2.5) and our aim is to identify this function in the most efficient manner. Once this is achieved (2.5) gives the scattered field everywhere. Using the expression D_q (corresponding to the plate equation) defined by

$$D_q = B\partial_{q_1}^4 - m\omega^2, \quad (2.6)$$

where the notation $\partial_{q_i} = \partial/\partial q_i$ has been adopted, and applying the operator $[1 +$

$(\omega^2 \rho)^{-1} D_q \partial_{q_3}]$ to (2.5) on $q_3 = 0$, leads to

$$\begin{aligned} & p^{sc}(q_1, 0) + D_q \eta^{sc}(q_1, 0) \\ &= -\rho \omega^2 \int_{-a}^a \eta^{sc}(x_1, 0) [p^G + D_q \eta^G](x_1, 0; q_1, 0) dx_1 \end{aligned} \quad (2.7)$$

$$= \frac{B}{2\pi} \int_{-a}^a \eta^{sc}(x_1, 0) dx_1 \times \int_{-\infty}^{\infty} \left[k^4 - \frac{m\omega^2}{B} - \frac{i\omega^2 \rho}{\gamma_0 B} \right] e^{ik(x_1 - q_1)} dk \quad (2.8)$$

for $|q_1| < a$. The integral on the right-hand side of (2.8) is formally divergent, but can be interpreted in the context of generalised functions. One could also arrive at (2.8) by applying transforms directly to the governing equation and boundary conditions. However in some circumstances, for instance cavity-backed finite elastic plates set into a baffle, the integral equation approach is more versatile: the Green's function contains a large amount of information regarding the problem geometry. With this in mind we have pursued the integral equation approach in more detail.

Two types of forcing are considered here: incident plane waves and local plate excitation. In the case of wave incidence, the left-hand side in the above equation is equal to $-(p^{in} + D_q \eta^{in})$. For line forcing at the centre of the plate the left-hand side becomes $F_0 \delta(q_1/a)$, and for line moment forcing it becomes $G_0 \delta'(q_1/a)$. For plane wave incidence, the incident pressure wave is taken as

$$p^{in}(q_1, q_3) = A[e^{i(kq_1 + \gamma_0 q_3)} + e^{i(kq_1 - \gamma_0 q_3)}], \quad (2.9)$$

where

$$k = k_0 \sin \theta_i \quad (2.10)$$

is the incoming wavenumber. This corresponds to the field produced by a pressure wave incident upon a defect-free rigid plate and its reflection from the plate. The corresponding displacement field therefore vanishes on the elastic plate, leading to

$$-[p^{in} + D_q \eta^{in}](q_1, 0) = -2Ae^{ikq_1} \quad (2.11)$$

for $|q_1| < a$.

Each applied incident field is split into two subproblems, one that is even in x and one that is odd in x . The unknown displacement along the plate is expanded as a series in a set of functions that automatically satisfy the clamped conditions $\eta(\pm a, 0) = \eta'(\pm a, 0) = 0$. The appropriate expression, in which the factor $4a^4/B$ is inserted merely for convenience, is

$$\eta^{sc}(x_1, 0) = \frac{4a^4}{B} \sum_{n=1}^{\infty} (a_n^{(e)} \psi_n^{(e)}(x_1/a) + a_n^{(o)} \psi_n^{(o)}(x_1/a)), \quad (2.12)$$

where the expansion functions ψ_n , in the even case, are

$$\psi_n^{(e)}(x) = \begin{cases} \cos[n \cos^{-1}(1 - x^2)^2] & \text{for } n \text{ odd,} \\ (1 - x^2) \cos[(n - 1) \cos^{-1}(1 - x^2)^2] & \text{for } n \text{ even.} \end{cases} \quad (2.13)$$

in $0 \leq x \leq 1$. For negative x these are extended as even functions of x . In the odd case

$$\psi_n^{(o)}(x) = \begin{cases} i \sin[(n + 1) \cos^{-1}(1 - x^2)^2] & \text{for } n \text{ odd,} \\ i(1 - x^2) \sin[n \cos^{-1}(1 - x^2)^2] & \text{for } n \text{ even.} \end{cases} \quad (2.14)$$

in $0 \leq x \leq 1$. These are extended as odd functions of x for negative x . The terms for n odd in these expansion functions are effectively Chebyshev polynomials. Crucially, they contain the correct edge behaviour in their argument and they are relatively easily generalised to account for more general edge conditions such as those suggested by [11].

The even terms in n are also similar to Chebyshev polynomials; their inclusion is vital as they contain the edge behaviour $O(1-x^2)^3$ as $x \rightarrow \pm 1$ that is omitted from the odd terms. This combination of expansion functions that contain the edge behaviour explicitly and are related to Chebyshev polynomials leads to very rapid numerical convergence. The expansion functions chosen here form a complete set (see Appendix B) and are designed to solve elastic plate problems involving the clamped edge conditions.

The integral equation (2.8) is split into even and odd subproblems. The even subproblem is solved by multiplying (2.8) by $\psi_m^{(e)}(q_1/a)$ and integrating from $-a$ to a , as well as expanding the scattered displacement on the plate. For an incoming wave of the form (2.11), this leads to

$$\begin{aligned} -\pi A \int_{-1}^1 \cos(kaq_1) \psi_m^{(e)}(q_1) dq_1 &= \sum_{n=1}^{\infty} a_n^{(e)} \int_{-\infty}^{\infty} \int_{-1}^1 \int_{-1}^1 \psi_m^{(e)}(q_1) \psi_n^{(e)}(x_1) \times \\ &\times e^{il(x_1-q_1)} \left[l^4 - (ak_p)^4 - \frac{i(ak_p)^6 \epsilon_c}{ak_0[(ak_0)^2 - l^2]^{\frac{1}{2}}} \right] dx_1 dq_1 dl \end{aligned} \quad (2.15)$$

The procedure for the odd subproblem is identical. The odd and even subproblems are completely separate. An alternative approach might be to substitute the expansion (2.12) directly into the plate equation, but one then has to incorporate the pressure term correctly, which is most directly achieved using transforms. In many circumstances the integral equation approach, although apparently unwieldy, incorporates a Green's function for the model geometry thereby building in a large amount of subsidiary details.

The square root in the integral has the same branch cut as γ_0 previously. For centred line force excitation, only the even expansion functions are required and the left-hand side becomes $\pi F_0/2$. For centred line moment excitation, only the odd expansion functions are required, and the left hand side is just $-\pi i c_m G_0$ where $c_m = m$ when m is even and $m + 1$ when m is odd. One advantage of the present approach is the simplicity with which different incident fields or localised excitations are incorporated: they just alter the left-hand side of (2.15) and its counterpart for the odd subproblem.

Integral equations involving square root singular edge behaviour can be solved using expansion functions that lead naturally to Bessel functions. These arise from the inner integrals with respect to x_1 and q_1 that can be done exactly [16,17]. The slowly convergent portions of the remaining l -integral are evaluated explicitly, thus leading to a fast numerical scheme. Adopting a similar approach here requires calculating triple integrals, a somewhat inefficient and tedious numerical procedure. Hence an alternative approach is adopted that utilises the properties of the dispersion relation, Fourier transforms and generalised functions to simplify the integrals. We temporarily drop the superscript (e) as similar calculations hold for the odd subproblem. To ease the notation we consider each term in the square brackets in succession and evaluate the integral with respect to l . For the first term, this integral is

$$\int_{-\infty}^{\infty} l^4 e^{il(x_1-q_1)} dl = 2\pi \delta^{(4)}(x_1 - q_1); \quad (2.16)$$

that is the fourth derivative of the delta function. Hence the corresponding part of the triple integral is simply

$$I_{mn}^{(1)} = 2\pi \int_{-1}^1 \psi_m''(x_1) \psi_n''(x_1) dx_1 \quad (2.17)$$

where we have integrated by parts twice and used the edge condition. This integral is

very easy to calculate numerically. The second integral leads to

$$I_{mn}^{(2)} = 2\pi \int_{-1}^1 \psi_m(x_1) \psi_n(x_1) dx_1, \quad (2.18)$$

which is, if anything, even simpler. The third Fourier integral is

$$\int_{-\infty}^{\infty} \frac{1}{(l_0^2 - l^2)^{\frac{1}{2}}} e^{il(x_1 - q_1)} dl = \pi H_0^{(1)}(l_0|x_1 - q_1|), \quad (2.19)$$

where the Hankel function is determined by the branch cut that has been taken. Thus

$$I_{mn}^{(3)} = \pi \int_{-1}^1 \int_{-1}^1 H_0^{(1)}(k_0 a|x_1 - q_1|) \psi_m(q_1) \psi_n(x_1) dx_1 dq_1. \quad (2.20)$$

In addition, temporarily replacing $|x_1 - q_1|$ by $|x_1 - q_1 + l|$ (which will be required later), this last integral may be rewritten as

$$\begin{aligned} I_{mn}^{(3)} &= \frac{\pi}{2} \int_0^2 [H_0^{(1)}(k_0 a|s + l|) + H_0^{(1)}(k_0 a|s - l|)] ds \times \\ &\times \int_{-2+s}^{2-s} \psi_m\left(\frac{1}{2}(t - s)\right) \psi_n\left(\frac{1}{2}(t + s)\right) dt. \end{aligned} \quad (2.21)$$

For the $l = 0$ case considered here, the two Hankel functions have the same argument. Isolating the Hankel functions leads to a more efficient numerical procedure. All the integrals have now been transformed to single or double integrals over finite ranges.

This procedure will work whenever the integrand has the factors k and $(k_0^2 - k^2)^{\frac{1}{2}}$ corresponding to differentiation with respect to x or y in the boundary condition on the plate. The former will naturally introduce delta functions and the latter will introduce Hankel functions.

The governing equation (2.15) may be rewritten as an infinite set of linear equations

$$b_m^{(e)}(ka) = \sum_{n=1}^{\infty} K_{mn}^{(e)} a_n^{(e)}, \quad (2.22)$$

for $m = 1, \dots, \infty$, where the left-hand side terms, which depend on the incident wavenumber, are given by

$$b_m^{(e)}(ka) = -\pi A \int_{-1}^1 \cos(kaq_1) \psi_m^{(e)}(q_1) dq_1 \quad (2.23)$$

for incident plane waves, by a similar integral for point irradiation, by $\pi F_0/2$ for line force and by $-\pi i c_m G_0$ for moment forcing. The right-hand side factors are given by

$$K_{nm}^{(e)} = I_{mn}^{(e)(1)} - (ak_p)^4 I_{mn}^{(e)(2)} - \frac{i(ak_p)^6 \epsilon_c}{ak_0} I_{mn}^{(e)(3)}. \quad (2.24)$$

Truncating this set of equations, and its counterpart for the odd subproblem, at some finite order N will give an approximate, but arbitrarily accurate (depending on the order of the truncation) solution to the original problem. Noting the symmetry with respect to m and n means that even for relatively large N , one need not evaluate an undue number of the K_{mn} . Typically, even for rather large $k_0 a$, we did not require $N > 15$.

Our primary objective is to identify the far-field behaviour of the scattered field. This is obtained by expanding the double integral in (2.5) for large $|\mathbf{q}|$. Taking the far-field variable as

$$\mathbf{q} = r(-\sin \phi, \cos \phi), \quad (2.25)$$

and using a steepest-descent approach gives

$$p^{sc}(r, \phi) \sim \left(\frac{2}{\pi r k_0} \right)^{\frac{1}{2}} G(\phi) e^{i(k_0 r - \frac{\pi}{4})} \quad (2.26)$$

for $k_0 r \gg 1$. The far-field directivity $G(\phi)$ is given by

$$G(\phi) = \frac{\rho \omega^2}{2i} \int_{-a}^a \eta^{sc}(x, 0) e^{ik_0 x_1 \sin \phi} dx_1, \quad (2.27)$$

which reduces in the even subproblem to

$$G^{(e)}(\phi) = -\frac{2i(k_p a)^6}{k_0 a} \epsilon_c \sum_{n=1}^{\infty} a_n^{(e)} \int_{-1}^1 \psi_n^{(e)}(x_1) \cos(ak_0 x_1 \sin \phi) dx_1. \quad (2.28)$$

together with a similar expression for the odd subproblem (replacing the cosine with a sine). The total directivity $G(\phi)$ the sum of the even and odd expressions. The coefficients $a_n^{(e)}$ depend on the type of forcing adopted and are the solutions of (2.22).

3. Results

The primary applications of the approach taken above are to scattering problems in underwater acoustics. As described in the introduction for lossless plates we have three parameters at our disposal: ϵ , M and $k_0 a$. For steel plates immersed in water, $\epsilon = 0.134$, while for aluminium plates in water, $\epsilon = 0.4$. The Mach number M will take the values 0.8 and 1.5 in the figures. The remaining parameter $k_0 a$ is a ratio of the lengthscale of the incident irradiating field to that of the finite plate; for the results presented here we take $k_0 a$ between .01 and 20. The amplitude of the incoming plane wave, A , is taken to be unity.

3.1. ‘Light’ fluid loading

In this section, we are interested in the limit $M = O(1)$, but not very close to 1. The fluid loading is hence light. For $M > 1$ we expect beam formation along the critical Mach angles defined by $\phi^M = \pm \sin^{-1}(M^{-1})$. In this limit the elastic plate is excited by an incident wave that generates flexural plate waves. If the fluid were absent, these would propagate along the plate with the *in vacuo* wave speed associated with k_p . Crucially the effect of adding a small amount of fluid loading is to introduce a small imaginary component to the wavenumber k_p ; thus the wave ‘leaks’ energy into the fluid. Moreover this energy is directed along the Mach angles. The leaky waves generated by interaction with the edge only attain their fully developed form when $k_0 a \sim O(1/\epsilon)$. Hence, provided the plates are long enough, the dominant acoustic directivity is along the rays along the Mach angles. When $O(\epsilon) < M < 1$, the plate waves are subsonic and beaming does not occur. If M is very close to 1, or $M = O(\epsilon)$, fluid loading effects are significant and the asymptotic approaches used here are not valid.

It is perhaps worth noting that one can adopt the useful approximation of solving the elastic plate problem in isolation from the fluid loading as in [18]. In terms of the numerical procedure adopted here, this drops the term $I_{mn}^{(3)}$ from the kernel function (2.24). The elastic plate solution is then used to drive the resulting fluid problem and this leads to highly accurate results away from resonances. Indeed following the approach of [9] allows analytical results to be found and these are now used to verify our numerical

approach. Away from resonance we solve

$$B \frac{\partial^4 \eta^{sc}}{\partial x_1^4} - m\omega^2 \eta^{sc} = -p^{in}; \quad (3.1)$$

that is, for $\epsilon \ll 1$ and when fluid loading is insignificant, the coupling term to the fluid pressure is dropped. For an incident plane wave the resulting plate deformation is

$$\begin{aligned} \eta^{sc}(x_1, 0) = & \frac{2A}{B(k_p^4 - k^4)} \left[e^{ikx_1} + (ka \cos k_p a \sin ka - k_p a \sin k_p a \cos ka) \frac{\cosh k_p x_1}{k_p a D(k_p a)} \right. \\ & - (ka \cosh k_p a \sin ka + k_p a \sinh k_p a \cos ka) \frac{\cos k_p x_1}{k_p a D(k_p a)} \\ & + (ka \cos ka \sin k_p a - k_p a \sin ka \cos k_p a) \frac{i \sinh k_p x_1}{k_p a F(k_p a)} \\ & \left. + (k_p a \sin ka \cosh k_p a - ka \cos ka \sinh k_p a) \frac{i \sin k_p x_1}{k_p a F(k_p a)} \right]. \quad (3.2) \end{aligned}$$

This somewhat lengthy formula contains terms in the denominator that can, for some values of $k_p a$, be zero; this corresponds to a resonance. Resonance occurs at the zeros of

$$D(k_p a) = \cosh k_p a \sin k_p a + \sinh k_p a \cos k_p a \quad (3.3)$$

and of

$$F(k_p a) = \sinh k_p a \cos k_p a - \cosh k_p a \sin k_p a. \quad (3.4)$$

Figure 2 shows the plate displacement, $\eta^{sc}(x, 0)$, for $M = 1.5$ and $k_0 a = 10$ for both the numerical and analytical solutions; $x \equiv x/a$ in the figures. For $\epsilon = .134$ the real part is virtually indistinguishable from (3.2). For relatively large values of $k_0 a$, such as 10, one might expect that the numerical procedure would require many expansion functions and become inefficient. However, the choice of expansion functions that has been made here leads to an efficient procedure: for $k_0 a = 10$ the truncation value N was perhaps conservatively taken to be 10. The relative difference between the power calculated for $N = 10$ and $N = 15$ is 0.01%.

Figure 2

The truncation value $N = 10$ was used for all the calculations in §3. The far field directivity $|G(\phi)|^2$ for normal incidence is shown in figure 3 and demonstrates beaming along the Mach angles shown by the straight lines in the figure. Note that the beams are displaced slightly from the Mach angles due to the effect of the main lobe. The directivity $G(\phi)$ driven by the *in vacuo* solution may be evaluated explicitly using (3.2) and (2.27). For $k_p a \gg 1$ this is

Figure 3

$$\begin{aligned} G(\phi) \sim & -\frac{2i\epsilon_c (k_p a)^2}{k_0 a} \left\{ \frac{\sin(k_0 a \sin \phi)}{k_0 a \sin \phi} \right. \\ & \left. - \frac{1}{2(\cos k_p a + \sin k_p a)} \left[\frac{\sin(k_p a + k_0 a \sin \phi)}{k_p a + k_0 a \sin \phi} + \frac{\sin(k_p a - k_0 a \sin \phi)}{k_p a - k_0 a \sin \phi} \right] \right\} \quad (3.5) \end{aligned}$$

For brevity we give only the expression for normal incidence ($k = 0$). For the parameters taken in figure 3, this expression, with $\epsilon = 0.134$, is almost indistinguishable from the full line curve. The first term is simply the well-known solution for a rigid plate with wave forcing for $\eta(x, 0)$ along a finite region (that is ignoring the edges and the elasticity of the plate). This generates the dominant lobe along $\phi = 0$. The two smaller beams close to the Mach angles are driven by the other terms and are generated by plate waves that are driven by the wave interaction with the edges. There are other smaller terms that can be incorporated; the resulting directivity for $\epsilon \ll 1$ is indistinguishable from that generated

numerically. These formulae also hold for viscoelastic plates with similar accuracy: the effect of introducing δ is to reduce η and the magnitude of the acoustic response, so in some regards the extra damping induced is equivalent to increasing the fluid loading. For non-normal incidence, one would expect a lobe driven by the plate in the absence of edge effects together with two lobes due to the leaky waves. However the main lobe and one of the leaky beams almost invariably interfere with each other tending to create a single beam that is not predominantly in one or the other of the above directions. For $\theta_i = \pi/12$, the directivity is shown in figure 4 for $M = 1.5, \epsilon = 0.134, \delta = 0$ together with the directivity generated by the *in vacuo* solution. This can of course be checked using a minor generalisation of (3.5).

Figure 4

The figures above have $M > 1$; in these cases the *in vacuo* results provide surprisingly accurate results even for relatively large ϵ . For $M < 1$ this is not the case, and the *in vacuo* results are only accurate for $\epsilon \ll 1$. Figure 5 show the directivities for $k_0 a = 10, M = 0.8$ for $\theta_i = \pi/4, \epsilon = 0.134$ and $\delta = 0, 0.2$. The *in vacuo* case is also shown and is given by a generalisation of (3.2). The main response is now along $\phi = -\pi/4$. There are several small peaks whose positions are picked out by the *in vacuo* solution, but the magnitude of the peaks is not accurately found. The inaccuracy of the *in vacuo* solution is to be expected as M decreases: the factor $\epsilon_c k_p^6/k_0$ multiplies the fluid loading term and for fixed k_0 , the effect of decreasing M is to increase k_p and thus the magnitude of the $\epsilon k_p^6/k_0$ factor also increases. The picture for point source irradiation is very similar.

Figure 5

The values used in the figures in this section are not close to resonance. If, however, we approach a resonance, near say $k_0 a = 8.2467$, (3.2) needs to be corrected. As it happens, resonance in this light loading limit is a relatively frequent occurrence. For instance, for $M = 1.5$, there are 9 resonant frequencies in the range $0 < k_0 a < 21$.

3.2. Asymptotic results for wide plates

One might naturally wonder how a numerical scheme such as the one proposed in this paper fares near the resonance values that were explicitly avoided in the previous section. Indeed this provides a reasonably good test of the proposed scheme. Thus the purpose of this section is to derive the asymptotic acoustic response and plate displacement near to resonance, and to compare these with the numerical results. In addition a useful analytic approximation is derived.

We consider the useful asymptotic limit of a wide strip, for which the ratio of a typical wavenumber to the width of the plate is large, i.e. $k_0 a \gg 1$ for light fluid loading, and $Ka \gg 1$ for heavy loading. In this limit one can initially treat each plate edge independently and then look at the effect of the diffracted waves generated by one edge upon the other and vice-versa. Thus one can separate the original problem into a sequence of semi-infinite problems that can each be solved explicitly using Fourier transforms and the Wiener–Hopf technique. This can be continued and used as the basis of a numerical method, as in [10]. We shall adopt an *ad hoc* procedure here which could be formalised as in [19], where the equivalent membrane problem is solved and also used to treat normal incidence. More general forcings, however, lead to considerable analysis involving sum splits; for such loadings the numerical method described in this paper is particularly useful.

We consider lossless plates ($\epsilon_c = \epsilon$) and normal incidence, in which case the incident field is

$$p^{in}(x_1, x_3) = e^{-ik_0 x_3}, \quad (3.6)$$

and the total field is split into reflected and scattered pieces. For convenience the reflected

field is chosen to make the plate unforced. Hence

$$p^{total} = e^{-ik_0x_3} + Re^{ik_0x_3} + p^{sc}, \quad (3.7)$$

where R is

$$R = \frac{ik_0 + \epsilon k_p^2/k_0}{ik_0 - \epsilon k_p^2/k_0}. \quad (3.8)$$

Thus insofar as the scattered field is concerned (dropping the *sc* superscript henceforth), the boundary conditions on $x_3 = 0$ are

$$\eta(x_1, 0) = -\frac{2}{Bk_p^4(1 + i\epsilon k_p^2/k_0^2)} \quad (3.9)$$

for $|x_1| > a$ and

$$B \left(\frac{\partial^4}{\partial x_1^4} - k_p^4 \right) \eta(x_1, 0) + p(x_1, 0) = 0 \quad (3.10)$$

for $|x_1| < a$. Defining the plate edges as new coordinate origins, we take $x = x_1 - a$ and $x' = x_1 + a$ we shall only use the x, x_3 coordinate system and utilise symmetry with respect to x_1 . Close to this origin the plate is, apparently, unaware of the other edge and we use the boundary conditions (3.9) and (3.10) (with x replacing x_1) for $x > 0$, and $x < 0$ respectively. The edge conditions that η and η' are continuous across $x = 0$ on $x_3 = 0$ are also used. This is a standard Wiener–Hopf problem and we define half range transforms in the usual manner as

$$\eta_+(k) = \int_{-\infty}^0 \eta(x, 0) e^{-ikx} dx, \quad T_-(k) = \int_0^{\infty} \left[\left(\frac{\partial^4}{\partial x^4} - k_p^4 \right) \eta(x, 0) + p(x, 0) \right] e^{-ikx} dx, \quad (3.11)$$

where the subscripts \pm denote that these functions are analytic in the upper and lower complex k -planes. The functional equation

$$\frac{T_-(k) - E(k)}{P_-(k)} - \frac{2P_+(0)}{Bk_p^4(1 + i\epsilon k_p^2/k_0^2)ik_-} = P_+(k)\eta_+(k) - \frac{2(P_+(k) - P_+(0))}{Bk_p^4(1 + i\epsilon k_p^2/k_0^2)ik_-} = 0 \quad (3.12)$$

is deduced, where the edge conditions have been used. The function $E(k)$ is a fourth order polynomial whose precise form is immaterial for what follows, and the functions $P_{\pm}(k)$ are described in Appendix A.

3.2.1. Light fluid loading

In the case of light fluid loading, the plate displacement is dominated by leaky waves with wavenumber k_l . This is a perturbation of the *in vacuo* plate waves incorporating a small imaginary component. There are also unattenuated subsonic flexural waves propagating with wavenumber K , and evanescent modes with wave number μ . The latter are a perturbation of the *in vacuo* exponential response ik_p . We can use (3.12) to deduce that the plate displacement in $x < 0$ is

$$\eta(x, 0) \sim \frac{2P_+(0)}{Bk_p^4(1 + i\epsilon k_p^2/k_0^2)} \left(\frac{(k_l - k_0)e^{-ik_lx}}{L_-(k_l)(k_l - K)(k_l - \mu)k_l} + \frac{(\mu - k_0)e^{-i\mu x}}{L_-(\mu)(\mu - K)(\mu - k_l)\mu} \right) \quad (3.13)$$

together with terms that are of asymptotically smaller order since $\epsilon \ll 1$ ($L_-(k)$ is defined in appendix A). The terms involving $\exp(-i\mu x)$ decay exponentially fast in x . However their inclusion ensures the plate displacement is accurately modelled at the plate edge $x = 0$. For convenience, the shorthand $\eta(x, 0) \sim -ce^{-ik_lx} + be^{-i\mu x}$ is used from now on.

It is important to realise that the plate displacement is of the same order as the

incoming wave. There is thus an identical contribution from the other edge, except that we replace x with $-x'$. The terms involving $e^{-i\mu x}$, $e^{i\mu x'}$ can be ignored when considering the interaction between the edges due to their rapid decay so each edge is struck only by an incident leaky wave. The reflected waves on the plate are once more of the same order as the incident field and $\eta(x, 0) \sim ae^{-ik_l x} + b'e^{-i\mu x}$ for $x < 0$. There is an identical contribution from the other edge, except that we replace x with $-x'$. Clearly all of these leaky plate waves induce extra contributions to η along $|x_1| > a$ so to assess the overall solution we remove these extra contributions to leading order. Thus we need to solve the boundary value problem

$$\eta(x, 0) = (c - a)e^{ik_l(x+2a)} \quad \text{for } x > 0 \quad (3.14)$$

together with

$$B \left(\frac{\partial^4}{\partial x^4} - k_p^4 \right) \eta(x, 0) + p(x, 0) = 0 \quad \text{for } x < 0. \quad (3.15)$$

The edge conditions that η and η' are continuous across $x = 0$ on $x_3 = 0$ are also required. The Wiener–Hopf technique can be utilised once more to give $\eta(x, 0)$ for $x < 0$. This is used in conjunction with (3.13) above and the contributions from the other edge to deduce that

$$\eta(x_1, 0) \sim \frac{2}{Bk_p^4(1 + i\epsilon k_p^2/k_0^2)} \left\{ 1 + \frac{2P_+(0)}{2k_l + CP_+(k_l)e^{2ik_l a}} \right. \\ \left. \left[2C \cos(k_l x_1) e^{ik_l a} + D \frac{\cos(\mu x_1) e^{i\mu a}}{\mu(\mu + k_l)} (2k_l(\mu + k_l) + (k_l - \mu)CP_+(k_l)e^{2ik_l a}) \right] \right\} \quad (3.16)$$

where C and D are

$$C = \frac{(k_0 - k_l)}{L_-(k_l)(K - k_l)(\mu - k_l)}, \quad D = \frac{(\mu - k_0)}{L_-(\mu)(\mu - K)(\mu - k_l)} \quad (3.17)$$

respectively. The relevant functions are evaluated in Appendix A.

A useful approximation is to perform the above steps assuming that $\eta(x, 0)$ can be represented by $Ae^{-ik_l x} + Be^{-i\mu x}$ for $x < 0$ and use this to solve the semi-infinite problems and identify A and B . Physically one might expect this to be an accurate approximation of the plate displacement. The crucial difference between this and the rigorous Wiener–Hopf solutions is that the acoustic coupling is assumed to be completely captured within the modified wavenumbers k_l , μ and thus that $L_-(k) \sim 1 + O(\epsilon^2)$, with $P_+(k)$ simply $(k + k_l)(k + \mu)$ in this light fluid loading limit. If this were the case, then (3.16) would reduce to (3.18). This is not asymptotically correct, unfortunately, as one can show that $L_-(k)$ is actually $1 + O(\epsilon)$. However the term multiplying ϵ is typically very small. The plate displacement deduced in this manner is

$$\eta(x_1, 0) \sim \frac{2}{Bk_p^4(1 + i\epsilon k_p^2/k_0^2)} \left(1 - \frac{\mu \cos k_l x_1 + 2ik_l \sin k_l a \cos(\mu x_1) e^{i\mu a}}{\mu \cos k_l a + ik_l \sin k_l a} \right). \quad (3.18)$$

This is an accurate approximation requiring only the zeros of the dispersion relation and can be generalised to point forcing, moments and general incident fields quite easily. The full Wiener–Hopf solution, on the other hand, requires complicated sum splits. This approximation is also excellent when the plate has complex bending stiffness.

The plate displacements given in (3.16), (3.18) are uniform approximations and hold at the resonant values of $k_p a$ when $D(k_p a) = 0$. They are also valid for plates with complex bending stiffness; in this case the loss factor effectively reduces the magnitude of the acoustic response at frequencies near resonance. In the near-resonance cases, as

discussed in [9], the acoustic response calculated via (2.27) is no longer $O(1)$ but is now $O(1/\epsilon)$; thus provided the plates are lossless one gets very large responses at these resonant values. We shall consider the resonance at $k_0 a = 8.246$, $M = 1.5$ for $\epsilon = 0.134$ and normally incident plane waves. The plate displacements, calculated using (3.18), for this situation are shown in figure 6 versus the numerical solution and the directivity is in figure 7. The agreement between the numerical results of η and its uniform approximation given by (3.18), using the light loading limits for μ and k_l (see Appendix A), is most impressive. The directivity is an order of magnitude larger than the directivities shown in figures 3, and the predominant response is along the Mach angles. The loss factor acts in a similar manner to increasing fluid loading; for δ small the acoustic response near resonance is no longer $O(1)$ but is the minimum of $O(1/\epsilon)$, $(1/\delta)$.

Figure 6**Figure 7**

To emphasise that the issue of edge conditions is not merely pedantic we digress to briefly consider the simply supported edge conditions, that is, $\eta = \eta'' = 0$ at the edges. One can perform similar analyses to look at the analytical *in vacuo* and wide strip approximations. For comparative purposes we take the *in vacuo* solution for the plate displacement with normally incident plane waves. For the simply supported case

$$\eta^{sc}(x_1, 0) = \frac{2A}{Bk_p^4} \left(1 - \frac{\cosh k_p x_1}{2 \cosh k_p a} - \frac{\cos k_p x_1}{2 \cos k_p a} \right). \quad (3.19)$$

This is compared with the real part of $\eta^{sc}(x_1, 0)$ for the clamped case near a resonant frequency of $D(k_p a)$ at $k_0 a = 12.955$, $\epsilon = 0.134$, $M = 1.5$ in figure 8. There is no common feature, and as the resonances are at completely different frequencies, the solutions are quite different.

Figure 8

3.2.2. Heavy fluid loading

So far the main emphasis has been upon light fluid loading for which substantial progress can be made utilising either *in vacuo* or wide strip approximations. Significant fluid loading effects occur when $\epsilon \ll 1$ and $M = O(\epsilon)$. However there is no great analytic simplification in that limit and one has to move to the heavy fluid loading limit where $M \ll \epsilon$ to make progress. The heavy fluid loading limit has been considered by several authors, for instance [8,20,21], and resonances may also occur in this limit. Differing scalings and definitions of heavy fluid loading have been adopted by different authors; here the scalings considered by [21] are used. Consequently we define heavy loading as the double limit when $\epsilon \ll 1$ and $M \ll \epsilon$, with structural inertia then vanishing to leading order in ϵ . This is equivalent to removing the term $I_{mn}^{(2)}$ in our kernel function: one is left with structural stiffness, fluid inertia and fluid pressure. In addition, this scaling renders the fluid almost incompressible. One can either implement the numerics directly using appropriate values of ϵ , M and $k_0 a$, or explicitly take the limits in advance, dropping the term $I_{mn}^{(2)}$ and taking the near incompressibility to mean that $k_0 a$ must be small. To compare with the results of [8] we take the latter course. In the analytical work γ_0 is replaced by $i|k|$.

The wide strip approximation is similar to that adopted in section 3.2.1 except that the dominant plate waves are now the subsonic plate waves with wavenumber K (which in this limit is approximately $k_p(\epsilon/M)^{\frac{1}{2}}$). For point forcing, [8] describes the asymptotic procedure in detail. The plate displacement is approximately

$$\eta(x_1, 0) \sim -\frac{1}{5BK^3} \left[\tan \frac{\pi}{10} + \cot \left(\frac{3\pi}{8} + Ka \right) \right] \cos Kx_1. \quad (3.20)$$

This plate displacement is shown in figure 9 for $k_0 a = .01$, $\epsilon = 0.134$, $M = 0.002$, $\delta = 0$, for both numerical (with and without the structural inertia term) and asymptotic results;

Figure 9

there is very good agreement. The discrepancy is due to the weak compressibility still contained within the numerics. The contribution from the structural inertia term within the full numerical evaluation was not negligible. However it has little effect upon the outcome which is dominated by the balance between structural stiffness and fluid inertia. The resonances and anti-resonances predicted by [8] are also detected. The far-field directivity in this very low frequency limit is effectively that of a point source.

4. A periodic array of finite plates

In this paper we have introduced a numerical method and verified that it provides an accurate and efficient solution method. Now, to demonstrate its utility, we briefly consider the problem of an array of finite plates in a rigid baffle.

Many structures have periodic stiffeners or ribs attached to provide additional rigidity. Such configurations are common in aircraft and marine structures, and hence scattering geometries involving periodic arrays have been extensively studied. Often these are taken to be point discontinuities and exact solutions can be found in terms of Fourier transforms; see for instance [22–24]. We are unaware of any study involving arrays of plates that explicitly takes into account the plate geometry. This is a canonical problem that involves plate interactions and edge effects. Arrays of cracks and gratings have been the subject of several studies in elastodynamics and in water-wave and acoustic theory; see for instance [14,25,26]. In those cases the periodicity allows a single integral equation to be deduced. Similar methods utilising periodicity are employed here. The crucial difference is that the expansion functions derived in this paper are required to satisfy the clamped edge conditions. In addition, the kernel function is rather more complicated due to the plate equation. However it can be significantly simplified thanks to various manipulations.

For brevity we shall consider normally incident plane waves. The extension to more general forcing such as oblique incidence is straightforward. We take $p^{in}(x_1, x_3) = A[e^{ikx_3} + e^{-ikx_3}]$. The geometry is shown in figure 10: the elastic plates lie along $x_3 = 0$ for $|x_1 + jd| < a$ and the rigid plates along $x_3 = 0$ for $|x_1 + jd/2| < -a + d/2$ where $j = 0, \pm 1, \pm 2, \dots$. The centres of neighbouring plates are separated by a distance d . The elastic plates satisfy equation (1.3) while the displacement η vanishes along the rigid baffle. The edge conditions are taken as the clamped conditions. The periodicity in the geometry implies periodicity in the scattered pressure and displacement fields, and so

$$p^{sc}(x_1 + jd, x_3) = p^{sc}(x_1, x_3), \quad \eta^{sc}(x_1 + jd, x_3) = \eta^{sc}(x_1, x_3). \quad (4.1)$$

Without loss of generality we consider the strip $|x_1| < d/2, 0 < x_3 < \infty$ with the elastic plate along $|x_1| < a$ for $x_3 = 0$. The periodicity is built in by utilising the periodic Green's function

$$p^{G\infty}(\mathbf{x}; \mathbf{q}) = \sum_{j=-\infty}^{\infty} p^G(x_1 + jd, x_3; q_1, q_3) \quad (4.2)$$

where $p^G(\mathbf{x}; \mathbf{q})$ is given by (2.4). This means that the periodic Green's function is an infinite sum of Hankel functions. Using the shift property of the delta function and the Fourier transform representation of the Green's function, an alternative representation can be derived. Applying Green's theorem within the strip yields the scattered pressure as

$$p^{sc}(\mathbf{q}) = -\rho\omega^2 \int_{-a}^a \eta^{sc}(x_1, 0) p^{G\infty}(x_1, 0; \mathbf{q}) dx_1. \quad (4.3)$$

The plate displacement is an unknown and is expanded using the $\psi_n^e(x_1)$, as defined

Figure 10

in (2.13) due to the even forcing. Thus we take $\eta^{sc}(x_1, 0)$ as the even part of (2.12) and henceforth suppress the superscript e . An integral equation for the unknown plate displacement follows from the manipulations described in section 2. This gives the simultaneous equations (2.22) once more, with a new kernel function

$$K_{mn} = 2\pi \sum_{j=-\infty}^{\infty} \int_{-1}^1 \int_{-1}^1 \psi_m(q_1) \psi_n(x_1) \left[\delta^{(4)}(x_1 + jd/a - q_1) - k_p^4 \delta(x_1 + jd/a - q_1) - \frac{i\omega^2 \rho}{2} H_0^{(1)}(k_0 a |x_1 + jd/a - q_1|) \right] dx_1 dq_1. \quad (4.4)$$

The integrals simplify in a similar fashion to §2 and the infinite sum only involves the last term as only the $j = 0$ term contributes in the others. Physically the plate displacement is coupled to that on the other plates via the fluid pressure term. The left-hand side of the simultaneous equations is given by (2.23) as before.

The far field for $q_3 \gg 1$ allows a representation in terms of Floquet modes of the form

$$p^{sc}(\mathbf{q}) = \sum_{j=-J}^J R_j \exp(i\gamma_{0j} q_3 - i\alpha_j q_1) \quad (4.5)$$

where J is the largest integer (modes for j larger than J are evanescent) such that $j \leq k_0 d/2\pi$, $\alpha_j = 2\pi j/d$, and $\gamma_{0j} = (k_0^2 - \alpha_j^2)^{1/2}$. Thus the propagating wave modes are in the directions $\theta = \pm \tan^{-1}(\alpha_j/\gamma_{0j})$. The R_j are given by

$$R_j = -\frac{4\epsilon_c (k_p a)^6}{k_0 a} \sum_{n=1}^{\infty} \frac{i}{d\gamma_{0j}} \int_{-1}^1 \psi_n(x) e^{i\alpha_j a x} dx. \quad (4.6)$$

In the case of the the incident field considered here, $R_{-j} = R_j$. The magnitude of the leading mode $|R_0|$ is shown in figure 11 versus $k_0 d$ for $\epsilon = .134$, $d/a = 6$, $M = 1.5$ and $\delta = 0$. The truncation $N = 5$ was sufficient to compute this figure. As one might expect, it picks up the resonance at the zero of $D(k_p a)$ in the interval considered. This forces the response there to be $O(1/\epsilon)$ greater than that elsewhere. This mode is considerably different from those associated with acoustic gratings where the various $|R_j|$ have sharp peaks and troughs associated with the cut-offs; for elastic plates these effects are masked by the dominant elastic effects.

Figure 11

As in section 3, one can obtain asymptotic results that provide useful checks upon the numerical results and provide simple analytic results. As noted above, each plate is coupled to the others in the array only via fluid coupling. Thus for frequencies away from resonance and for light fluid loading, the plates do not couple with one another and the plate displacement is simply given by (3.2) (with $\theta_i = 0$) to leading order. The explicit solutions for the R_j are therefore

$$R_j = -\frac{i\epsilon_c (k_p a)^2}{k_0 a d \gamma_{0j}} \left\{ \frac{\sin(\alpha_j a)}{\alpha_j a} - \frac{\sinh k_p a}{D(k_p a)} \left[\frac{\sin(\alpha_j + k_p) a}{k_p a + \alpha_j a} + \frac{\sin(\alpha_j - k_p) a}{k_p a - \alpha_j a} \right] - \frac{\sin k_p a}{D(k_p a)} \left[\frac{\sinh(i\alpha_j + k_p) a}{i\alpha_j a + k_p a} + \frac{\sinh(i\alpha_j - k_p) a}{i\alpha_j a - k_p a} \right] \right\}. \quad (4.7)$$

In this light fluid loading limit this is a close approximation, although it clearly fails near to resonance where similar corrections to those pursued in section 3.2.1 can be taken.

5. Reciprocity and Power

It is important to utilise analytical results as checks upon the numerical procedure wherever possible. For a single finite plate in a rigid baffle subjected to incident plane waves, both reciprocity and power balance theorems are used, and are both satisfied to a high degree of accuracy. The reciprocity relation states that

$$G(\phi, \theta_i) = G(\theta_i, \phi) \quad (5.1)$$

where the second argument of G in this equation denotes the angle of the incident plane wave. That is, the directivity evaluated along ϕ due to an incident plane wave from θ_i is the same as the directivity evaluated along θ_i due to an incident plane wave from ϕ . This relates two independent scattering problems; a derivation is contained in [27] together with earlier references. This is a necessary, but not sufficient, condition that demonstrates the accuracy of our procedure. It is automatically satisfied, as is power balance, by the numerical procedure of this paper and serves mainly as a consistency check on the numerical procedure itself rather than of the physics; a discussion of this aspect is contained in [17].

The power balance for lossless plates is given by

$$\frac{1}{2\pi} \int_{-\pi/2}^{\pi/2} |G(\phi)|^2 d\phi = -\text{Re} (G(-\theta_i)). \quad (5.2)$$

This follows from utilising the reciprocal theorem with one state taken to be the complex conjugate of the other. Taking the region over which the reciprocal theorem is applied to enclose the obstacle, the total time averaged power flow is zero, thus one can relate an integral involving the far field directivities to an integral along the plate which is easily evaluated. This is a useful check as it relates the integral of the directivity to the specific value along a ray. For the lossless plate, this condition is satisfied to an extremely high order of accuracy in the present numerical algorithm (8 decimal digits). However, it is not satisfied for viscoelastic plates due to the dissipation of energy within the plate.

For the periodic array we have considered, a power balance relation can be similarly derived in the form

$$\sum_{-J}^J \gamma_{0j} |R_j|^2 = -2k_0 \text{Re} (R_0). \quad (5.3)$$

The sum is taken over the propagating modes; once again this is satisfied to high accuracy.

6. Conclusion

A highly efficient and accurate numerical scheme has been developed to tackle wave scattering problems in structural acoustics. It is valid over a wide range of frequencies and parameter values. The scheme tackles finite problems via an integral equation approach. The unknown within the integral equation is expanded using functions that are explicitly designed to satisfy the edge conditions, and the numerical solution rapidly converges and without Gibbs' phenomenon to the solution (as may be checked when the asymptotic solutions are known). In addition this representation leads to simple expressions for the directivities and plate displacements. The idea of explicitly inserting the edge behaviour within the argument of a Chebyshev-like polynomial is not entirely new; it has a long history in elastodynamic scattering where expansions in $T_n(\sqrt{1-x^2})$ have considerable advantages. In those cases the Chebyshev polynomial terms are the eigenfunctions for Laplace's equation in the elliptic coordinates. However the advantages of using a

similar idea to incorporate more general edge behaviour has not been generally adopted. Such an approach has many virtues, not least the relative simplicity of the results and rapid convergence with few expansion terms required, due in part to the properties of Chebyshev approximation.

The aim here has been to thoroughly validate this numerical approach thoroughly using analytical results and to investigate both single and periodic arrangements of baffled plates. In the process, a useful approximation (3.18) is identified near resonant frequencies in the light fluid loading limit. Excellent agreement is obtained in both light and heavy fluid loading limits. Future work could use this method to analyse compliant coatings, plate interactions and other scattering configurations.

SGLS was funded at the Scripps Institution of Oceanography by a Lindemann Trust Fellowship administered by the English Speaking Union. RVC acknowledges an EPSRC Advanced Fellowship. Conversations with Prof. F. G. Leppington were helpful.

Appendix A. Factorisation

In the text a Wiener–Hopf method is utilised to solve the integral equations in an asymptotic manner for wide strips and lossless plates. The crux of this analysis is the factorisation of the kernel function

$$P(k) = k^4 - k_p^4 + \frac{\epsilon k_p^6}{ik_0 \gamma_0(k)} \quad (\text{A } 1)$$

into the product of functions analytic in the upper and lower complex k -planes respectively, that is, $P(k) = P_+(k)P_-(k)$. This particular function has been factorised by many authors, either in full or via asymptotic factorisations taking advantage of various limits [6–8]. Here an alternative factorisation is presented, which has the advantage of not requiring the calculation of zeros of high order polynomials inside the integrals that arise. It is also rather convenient when k_p has an imaginary component.

This factorisation is based upon splitting a new function $L(k)$ defined as

$$L(k) = \frac{P(k)(k^2 - k_0^2)}{(k^2 - K^2)(k^2 - \mu^2)(k^2 - k_l^2)} \quad (\text{A } 2)$$

into the product $L_+(k)L_-(k)$. The function $P(k)$ has, for $M > 1$, six zeros in the complex k -plane cut from $\pm k_0$ to $\pm k_0 \pm i\infty$. For lossless plates two are real with value $\pm K$ where $K > k_0$; these give rise in the physical domain to plate waves that are subsonic relative to the fluid wave speed. Two are at $\pm k_l$; for $\epsilon \ll 1$, these are the leaky zeros corresponding to the leaky waves in the physical domain which for $\epsilon \ll 1$ are in close proximity to the *in vacuo* wavenumbers $\pm k_p$. The final two are at $\pm \mu$; these are in the proximity of $\pm ik_p$ and lead to rapidly decaying modes. The effect of the loss factor is to add a small imaginary component to both K and k_l . These six zeros are obtained with the branch cuts taken to run from k_0 to $k_0 + i\infty$ and from $-k_0$ to $-k_0 - i\infty$; different choices of cuts may lead to various zeros moving onto different Riemann sheets or new zeros appearing; see [28]. For instance when $M < 1$ with the choice of cuts taken above, the leaky zeros move through the cuts and onto the lower Riemann sheet. When we later rotate the cuts onto $\pm k_0$ to $\pm i\infty$ these zeros reappear on the principal Riemann sheet; for $M < 1$ the position of the zeros $\pm k_l$ is evaluated with the branch cuts taken along the real axis. Thus $L(k)$ has no zeros; the apparent zeros introduced by the multiplicative factor $k^2 - k_0^2$ are in fact branch point singularities due to the factor $1/\gamma$ in $P(k)$. Moreover $L(k) \rightarrow 1$ as $|k| \rightarrow \infty$

and thus the factorisation

$$\log L_{\pm}(k) = \pm \frac{1}{2\pi i} \int_C \frac{\log L(z)}{z-k} dz \quad (\text{A } 3)$$

is used. For lossless plates the factorisation is performed as follows: the path C runs from $-\infty$ to $+\infty$ and is indented to pass below the branch point singularity that lies on the positive real axis and above that on the negative real axis. We now rotate the branch cut for γ_0 so that it runs from k_0 to $+\infty$ and $-k_0$ to $-\infty$. Wrapping the contour integral for $L_-(k)$ around the upper branch cut then gives

$$L_-(k) = \left(\frac{k_0 - k}{K - k} \right)^{\frac{1}{2}} \exp \left(-\frac{1}{2\pi i} \int_{k_0}^{\infty} \log \left| \frac{z^4 - k_p^4 - \epsilon k_p^6/k_0(z^2 - k_0^2)^{\frac{1}{2}}}{z^4 - k_p^4 + \epsilon k_p^6/k_0(z^2 - k_0^2)^{\frac{1}{2}}} \right| \frac{dz}{z-k} \right). \quad (\text{A } 4)$$

The presence of the apparent branch point singularities at $\pm K$ is to be expected. The zero at $+K$ now lies on the branch cut, although its influence is implicitly diminished by the choice of factors in $L(k)$. The factorisation of a function with similar behaviour in [29] leads to similar square root factors. The integral in (A 4) converges rapidly. Thus $P_-(k)$ is found from

$$L_-(k) = \frac{P_-(k)(k - k_0)}{(k - K)(k - \mu)(k - k_l)} \quad (\text{A } 5)$$

and by symmetry the function $L_+(k)$ is $L_-(-k)$. The function $P_+(0)$ is

$$P_+(0) = ik_p^2 \left(1 + \frac{i\epsilon k_p^2}{k_0^2} \right)^{\frac{1}{2}}. \quad (\text{A } 6)$$

It is perhaps not obvious that

$$P(\xi) = \left(\frac{K^2 - \xi^2}{k_0^2 - \xi^2} \right)^{\frac{1}{2}} (\xi^2 - \mu^2)(\xi^2 - k_l^2) \times \exp \left(-\frac{1}{2\pi i} \int_{k_0}^{\infty} \log \left| \frac{z^4 - k_p^4 - \epsilon k_p^6/k_0(z^2 - k_0^2)^{\frac{1}{2}}}{z^4 - k_p^4 + \epsilon k_p^6/k_0(z^2 - k_0^2)^{\frac{1}{2}}} \right| \frac{2z dz}{z^2 - k^2} \right). \quad (\text{A } 7)$$

and this formula acts as a check upon the split proposed here. For plates with non-zero loss factor the wavenumber K has a small imaginary part and no longer lies upon the branch cut; a similar argument to that pursued above can be adopted to simplify (A 3). For heavy fluid loading a useful limit is

$$K^{\frac{1}{2}} P_+(K) = \left(\frac{\epsilon k_p^6}{k_0} \right)^{\frac{1}{2}} (10)^{\frac{1}{2}} e^{3i\pi/8}, \quad (\text{A } 8)$$

$$P_+(0) = e^{3i\pi/4} \left(\frac{\epsilon k_p^6}{k_0^2} \right)^{\frac{1}{2}}, \quad (\text{A } 9)$$

(see [21]), and this is used in section 3.2.2. To use these formulae, we need the zeros K, k_l, μ of $P(k)$: they are found using a trivial adaption of the argument principle, as in [30]. Asymptotic formulae for the zeros are in [28]. In the light case, and with a minor change in notation, they are

$$K \sim k_0 \left(1 + \frac{\epsilon^2}{2M^4(M^4 - 1)^2} \right), \quad (\text{A } 10)$$

$$\mu \sim k_p \left(i - \frac{\epsilon}{4M(M^2 + 1)^{\frac{1}{2}}} \right), \quad (\text{A } 11)$$

$$k_l \sim k_p \left(1 + \frac{i\epsilon}{4M(M^2 - 1)^{\frac{1}{2}}} \right). \quad (\text{A } 12)$$

These results are naturally valid only for $M > 1$.

Appendix B. Completeness of the expansion functions

It is important to verify that the plate displacement can actually be represented by the expansion functions, and that the latter are hence complete. The expansion functions used in elasticity for crack problems by [16] and others may easily be shown to be complete. These functions are (to within a normalisation factor)

$$\phi_n = \begin{cases} \cos(n \sin^{-1} x) & \text{for } n \text{ odd,} \\ \sin(n \sin^{-1} x) & \text{for } n \text{ even} \end{cases} \quad (\text{B } 1)$$

on the interval $(-1, 1)$. The change of variable $x = \sin \theta$ maps the x -interval $(-1, 1)$ onto $(-\frac{\pi}{2}, \frac{\pi}{2})$. On this interval, the expansion functions are

$$\phi_n = \begin{cases} \cos n\theta & \text{for } n \text{ odd,} \\ \sin n\theta & \text{for } n \text{ even.} \end{cases} \quad (\text{B } 2)$$

This set of functions is complete on the interval $(-\frac{\pi}{2}, \frac{\pi}{2})$, since it corresponds to the usual Fourier sine expansion.

The set given by (2.13)–(2.14) requires more care. Any function f on $(-1, 1)$ may be decomposed into its odd and even parts f_o and f_e respectively, both defined on $(0, 1)$ and with $f'_e(0) = f_o(0) = 0$. The even expansion functions $\psi_e = \cos[n \cos^{-1}(1 - x^2)^2]$ with n odd map the interval $(0, 1)$ into $(0, \frac{\pi}{2})$. On this interval, the transformed even expansion functions are again $\cos n\theta$ for n odd. This set of functions is not complete on this: a complete set of cosines on this interval requires even n as well. However, picking the even cosines as extra expansion functions would remove the correct edge condition in the original variable x and hence introduce Gibbs' effects that would undermine the whole aim of the expansion functions. The additional functions $\psi'_e = (1 - x^2) \cos[n \cos^{-1}(1 - x^2)^2]$, which explicitly introduce terms of the form $(1 - x^2)^3$ near $x = \pm 1$, satisfy the appropriate boundary conditions, and project onto all the cosine functions (including the odd ones). This may be verified by calculating the integrals

$$\int_0^{\pi/2} \sqrt{\cos \theta} \cos n\theta \cos m\theta \, d\theta \quad (\text{B } 3)$$

for n odd, using 7.346 of [31]. Hence the set of expansion functions for the even part of f is complete. The issue of whether these expansion functions are orthogonal with respect to a particular weight function is irrelevant since orthogonality properties are never used.

The argument for the odd part of f is analogous. Hence the set of expansion functions (2.13)–(2.14) is complete, and in addition satisfies the appropriate clamped boundary condition.

REFERENCES

- [1] D. G. Crighton, "The 1988 Rayleigh medal lecture: fluid loading – the interaction between sound and vibration," *J. Sound Vib.* 133, 1–27 (1988).

- [2] M. C. Junger and D. Feit, *Sound, structures and their interaction*, Acoustical Society of America (1986), second edition.
- [3] F. G. Leppington, "Acoustic scattering by membranes and plates with line constraints," *J. Sound Vib.* *58*, 319–332 (1978).
- [4] M. S. Howe, "Scattering of bending waves by open and closed cracks and joints in a fluid-loaded elastic plate," *Proc. R. Soc. Lond. A* *444*, 555–571 (1994).
- [5] P. R. Brazier-Smith, "The acoustic properties of two co-planar half-plane plates," *Proc. R. Soc. Lond. A* *409*, 115–139 (1987).
- [6] P. A. Cannell, "Edge scattering of aerodynamic sound by a lightly loaded elastic half-plane," *Proc. R. Soc. Lond. A* *347*, 213–238 (1975).
- [7] P. A. Cannell, "Acoustic edge scattering by a heavily loaded elastic half-plane," *Proc. R. Soc. Lond. A* *350*, 71–89 (1976).
- [8] D. G. Crighton and D. Innes, "Low frequency acoustic radiation and vibration response of locally excited fluid-loaded structures," *J. Sound Vib.* *91*, 293–314 (1983).
- [9] F. G. Leppington, "Scattering of sound waves by finite membranes and plates near resonance," *Q. J. Mech. Appl. Math.* *29*, 527–546 (1976).
- [10] J. F. M. Scott, "Acoustic scattering by a finite elastic strip," *Phil. Trans. R. Soc. Lond. A* *338*, 145–167 (1992).
- [11] F. G. Leppington, E. G. Broadbent and K. H. Heron, "Acoustic radiation from rectangular panels with constrained edges," *Proc. R. Soc. Lond. A* *393*, 67–84 (1984).
- [12] R. V. Craster and S. G. Llewellyn Smith, "A class of expansion functions for finite scattering problems in structural acoustics," Submitted to *Journal of the Acoustical Society of America* (1997).
- [13] E. E. Ungar, "Damping of panels," in: *Noise and Vibration control*, edited by L. E. Beranek, chap. 14, Institute of Noise Control Engineering (1988).
- [14] R. Porter and D. V. Evans, "Wave scattering by periodic arrays of breakwaters," *Wave Motion* *23*, 95–120 (1996).
- [15] J. D. Achenbach and R. J. Brind, "Scattering of surface waves by a sub-surface crack," *J. Sound Vib.* *76*, 43–56 (1981).
- [16] F. L. Neerhoff and J. H. M. T. van der Hijden, "Diffraction of elastic waves by a sub-surface crack (anti-plane motion)," *J. Sound Vib.* *93*, 523–536 (1984).
- [17] R. V. Craster, "Scattering by cracks beneath fluid-solid interfaces," *J. Sound Vib.* *209*, 343–372 (1998).
- [18] D. G. Crighton, "Acoustic edge scattering of elastic surface waves," *J. Sound Vib.* *22*, 25–32 (1972).
- [19] I. D. Abrahams, "Scattering of sound by large finite geometries," *IMA J. Appl. Math.* *29*, 79–97 (1982).
- [20] I. D. Abrahams, "Scattering of sound by a heavily loaded finite elastic plate," *Proc. R. Soc. Lond. A* *378*, 89–117 (1981).
- [21] D. G. Crighton and D. Innes, "The modes, resonance and forced response of elastic structures under heavy fluid loading," *Phil. Trans. R. Soc. Lond. A* *312*, 295–342 (1984).
- [22] V. N. Evseev, "Sound radiated from an infinite plate with periodic inhomogeneities," *Soviet Phys. Acoust.* *19*, 226–229 (1973).
- [23] B. R. Mace, "Periodically stiffened fluid-loaded plates. I: response to convected harmonic pressure and free wave propagation," *J. Sound Vib.* *71*, 435–441 (1980).
- [24] B. R. Mace, "Periodically stiffened fluid-loaded plates. II: response to line and point forces," *J. Sound Vib.* *71*, 487–504 (1980).
- [25] Y. C. Angel and J. D. Achenbach, "Reflection and transmission of elastic waves by a periodic array of cracks," *J. Appl. Mech.* *52*, 33–41 (1985).
- [26] J. D. Achenbach and Z. L. Li, "Reflection and transmission of scalar waves by a periodic array of screens," *Wave Motion* *8*, 225–234 (1986).

- [27] T. H. Tan, "Reciprocity relations for scattering of plane elastic waves," *J. Acoust. Soc. Am.* *61*, 928–931 (1977).
- [28] D. G. Crighton, "The free and forced waves on a fluid-loaded elastic plate," *J. Sound Vib.* *63*, 225–235 (1979).
- [29] R. V. Craster and C. Atkinson, "Shear cracks in thermoelastic and poroelastic media," *J. Mech. Phys. Solids* *40*, 887–924 (1992).
- [30] R. V. Craster, "A canonical problem for fluid-solid interfacial wave coupling," *Proc. R. Soc. Lond. A* *452*, 1695–1711 (1996).
- [31] I. S. Gradshteyn and I. M. Ryzhik, *Table of Integrals, Series, and Products*, Academic Press, corrected and enlarged edn. (1980).

FIGURE CAPTIONS

FIGURE 1: Typical geometry, incident fields and forcing functions.

FIGURE 2: Real and imaginary parts of the plate displacement $B_1\eta^{sc}(x,0)/a^4$ versus x for $k_0a = 10$, $M = 1.5$, $\theta_i = 0$ and $\epsilon = 0., .01, .134, .4$ and $\delta = 0$, and for $\epsilon = .01, \delta = 0.2$. Of the two dot-dashed lines, the one with $\epsilon = 0.01$ is closer to the solid line; in fact its real part is indistinguishable from the $\epsilon = 0$ case.

FIGURE 3: The directivity $|G(\phi)|^2$ for $k_0a = 10$, $M = 1.5$, $\theta_i = 0$ and $\epsilon = 0.134$. The viscoelastic case with $\epsilon = 0.134, \delta = 0.2$ is also shown as are the Mach angles.

FIGURE 4: The directivity $|G(\phi)|^2$ for $\theta_i = \pi/12$, $k_0a = 10$, $M = 1.5$, $\epsilon = 0.134$ and $\delta = 0$. The directivity for fluid driven by the *in vacuo* solution is also shown, as are the line $\phi = -\pi/12$ and the Mach angles.

FIGURE 5: The directivities $|G(\phi)|^2$ for $k_0a = 10, M = 0.8, \theta_i = \pi/4, \epsilon = 0.134$ and $\delta = 0, 0.2$. The *in vacuo* case is also shown.

FIGURE 6: The real and imaginary parts of the plate displacement $B_1\eta^{sc}(x,0)/a^4$ versus x for $k_0a = 8.246$, $M = 1.5$, $\theta_i = 0$, $\epsilon = .134$ and $\delta = 0$. Also shown are the real and imaginary parts of the asymptotic result for a wide plate (3.18) which holds near resonance.

FIGURE 7: The directivity $|G(\phi)|^2$ for $k_0a = 8.246, M = 1.5$ for $\theta_i = 0, \epsilon = 0.134$ and $\delta = 0$. The Mach angles are also shown.

FIGURE 8: The real parts of the plate displacement $B_1\eta^{sc}(x,0)/a^4$ versus x for $k_0a = 12.955, M = 1.5, \theta_i = 0$ and $\epsilon = .134, \delta = 0$ for the simply supported and clamped edge conditions.

FIGURE 9: The real part of the plate displacement $B_1\eta^{sc}(x,0)/a^4$ versus x (in $[0,1]$) for point force loading with $k_0a = 0.01, M = 0.002$ and $\epsilon = .134, \delta = 0$. Also shown are the plate displacement for $I_2 = 0$ and the heavy loading asymptotic result (3.20).

FIGURE 10: Geometry for the periodic array of plates with a normally incident wave field.

FIGURE 11: Modulus of the zero propagating wave mode $|R_0|$ versus k_0d , for $\epsilon = 0.134$,

$d/a = 6$, $M = 1.5$ and $\delta = 0$. The dotted lines correspond to cut-on values of the periodicity. The dashed line is the first even resonance at $k_p a \approx 3.5475$.

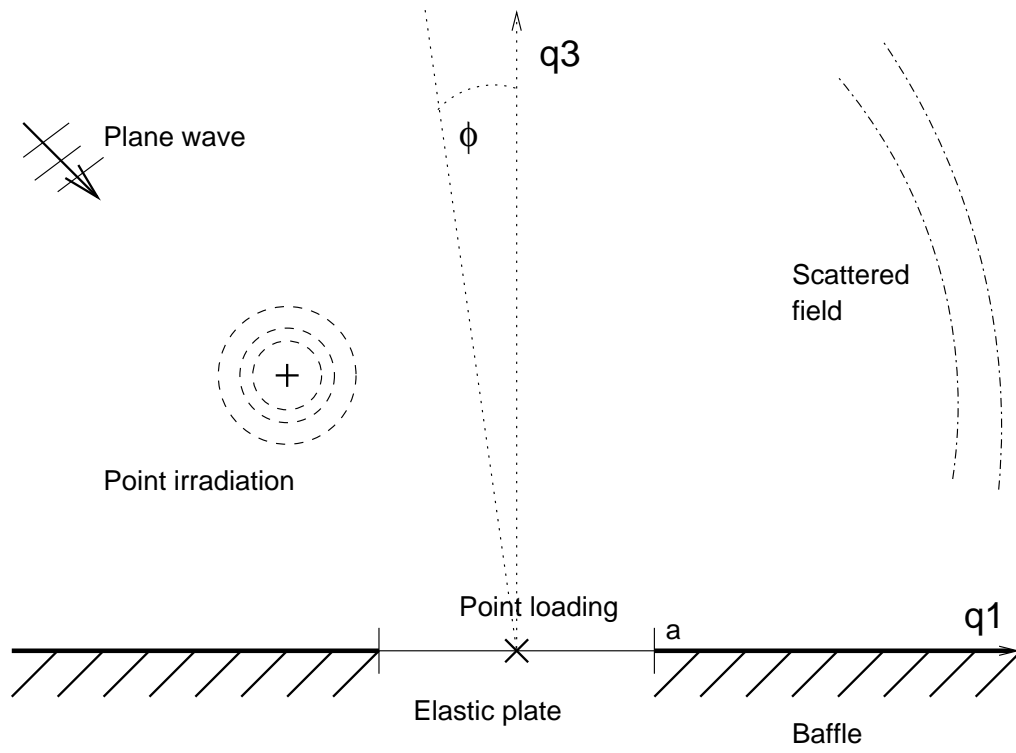


FIGURE 1.

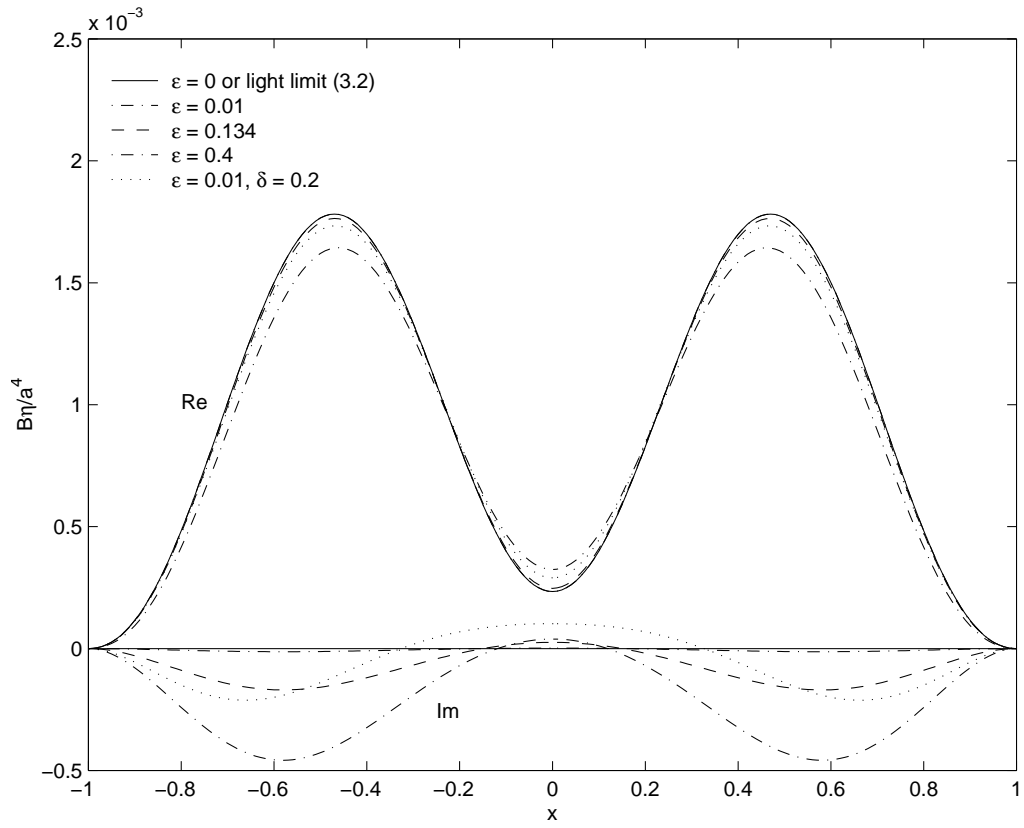


FIGURE 2.

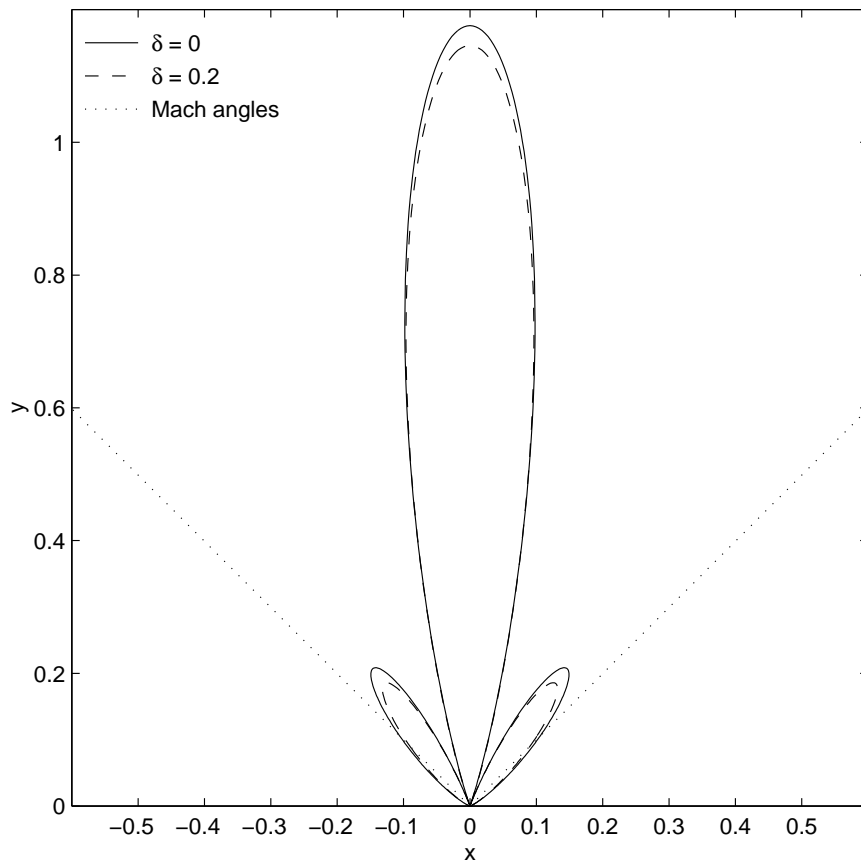


FIGURE 3.

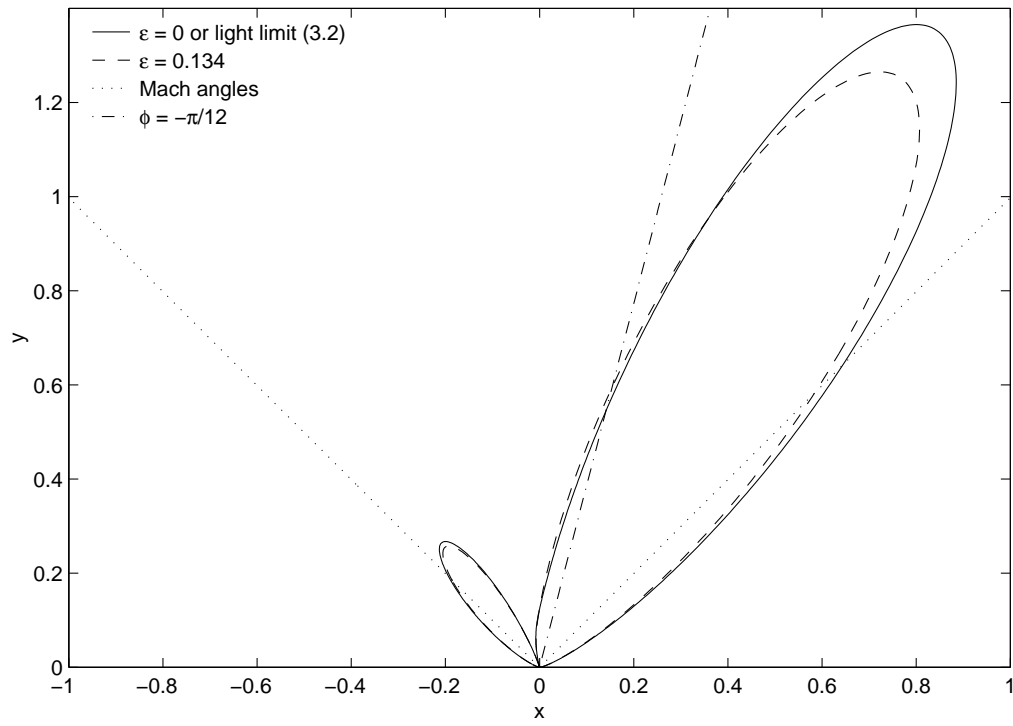


FIGURE 4.

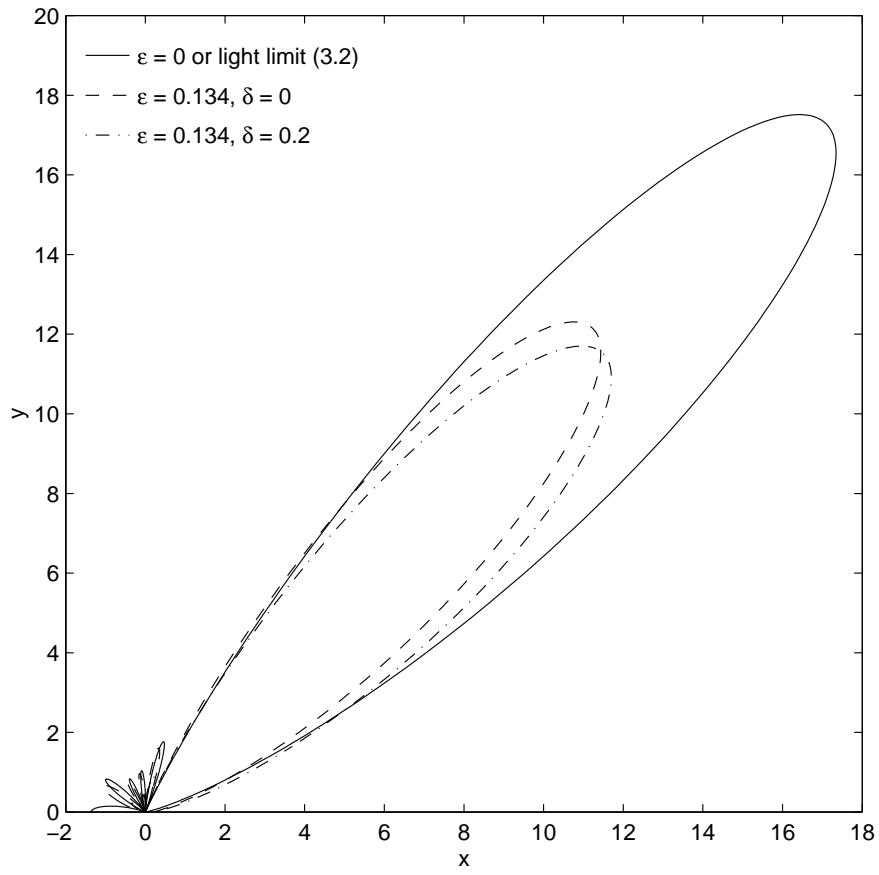


FIGURE 5.

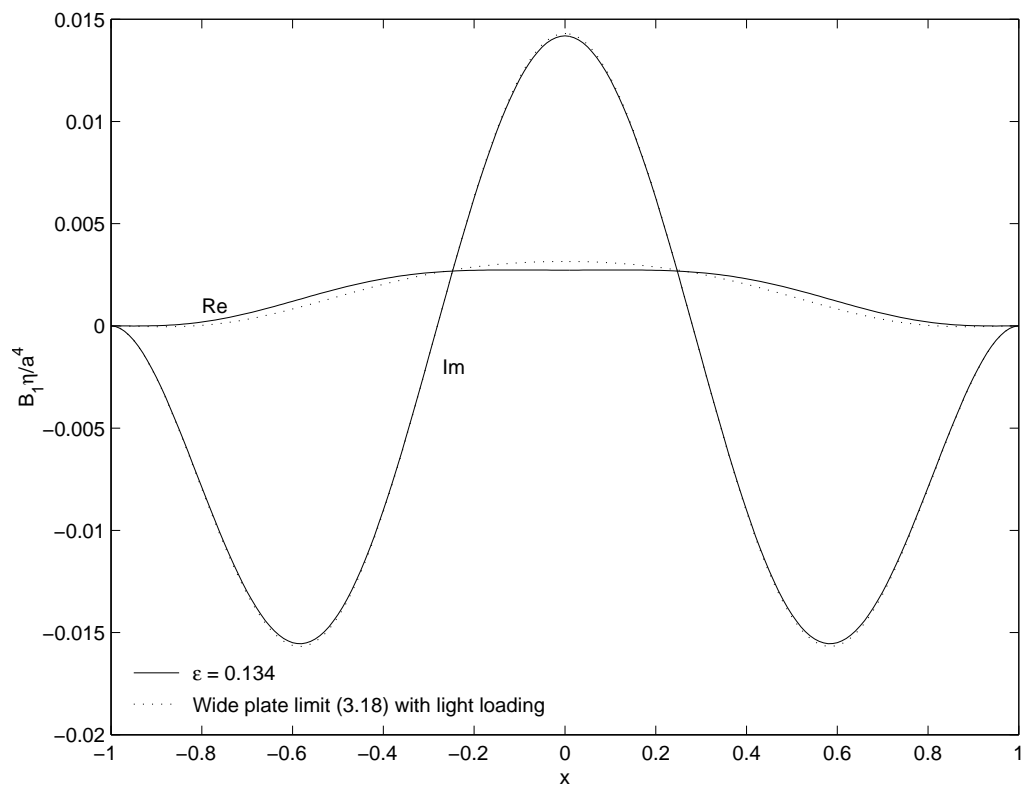


FIGURE 6.

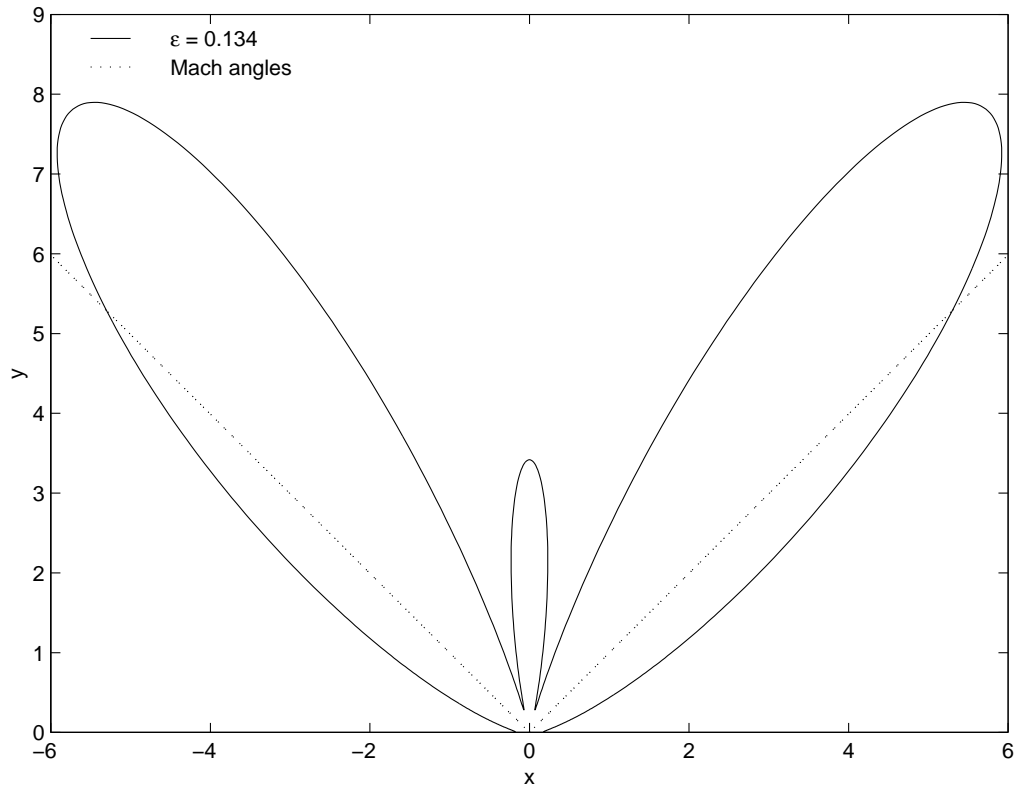


FIGURE 7.

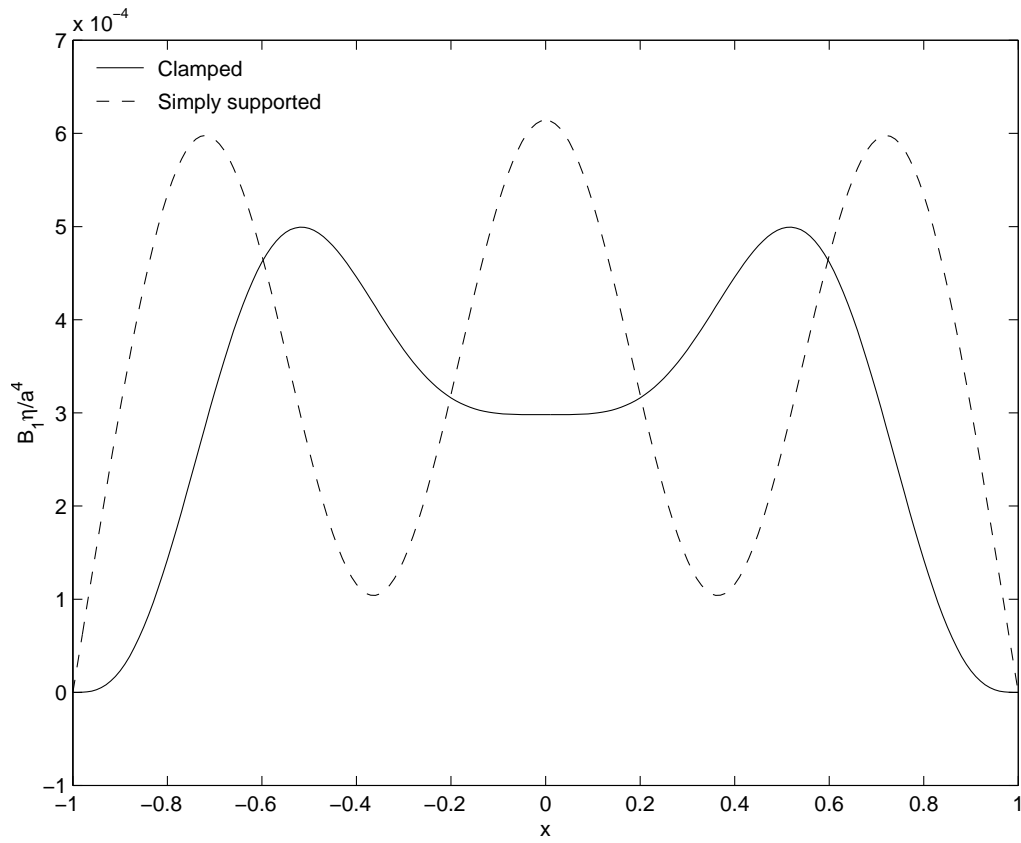


FIGURE 8.

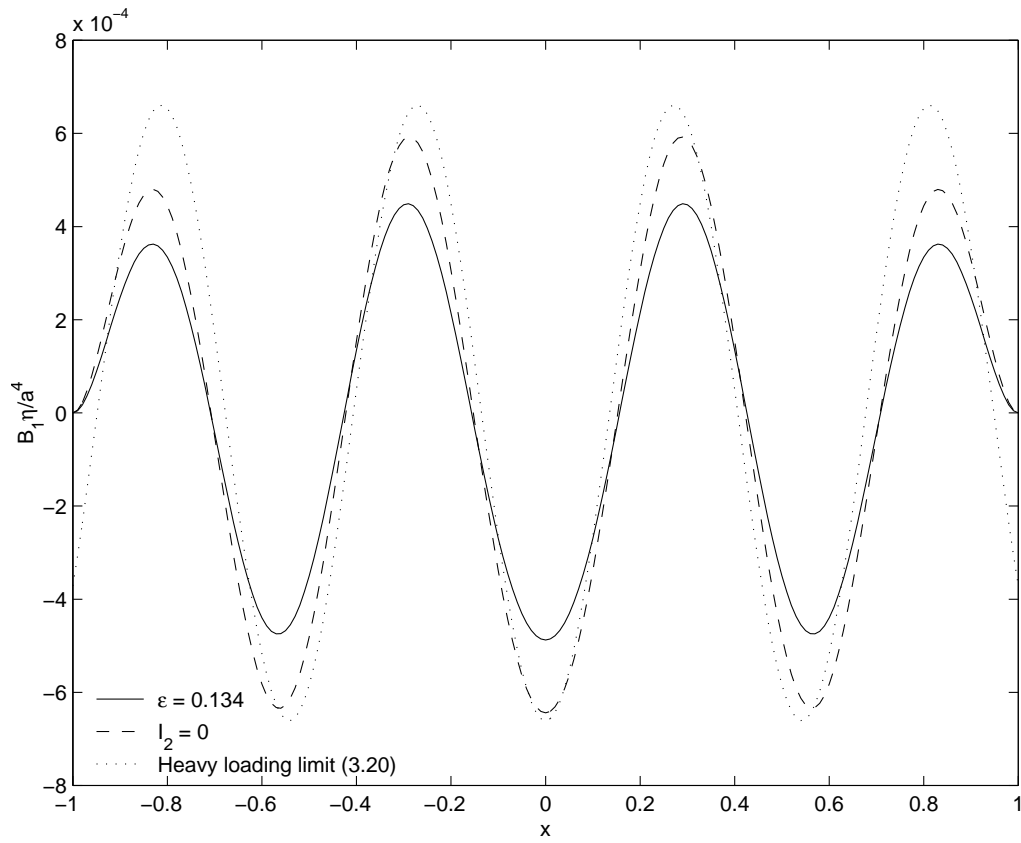


FIGURE 9.

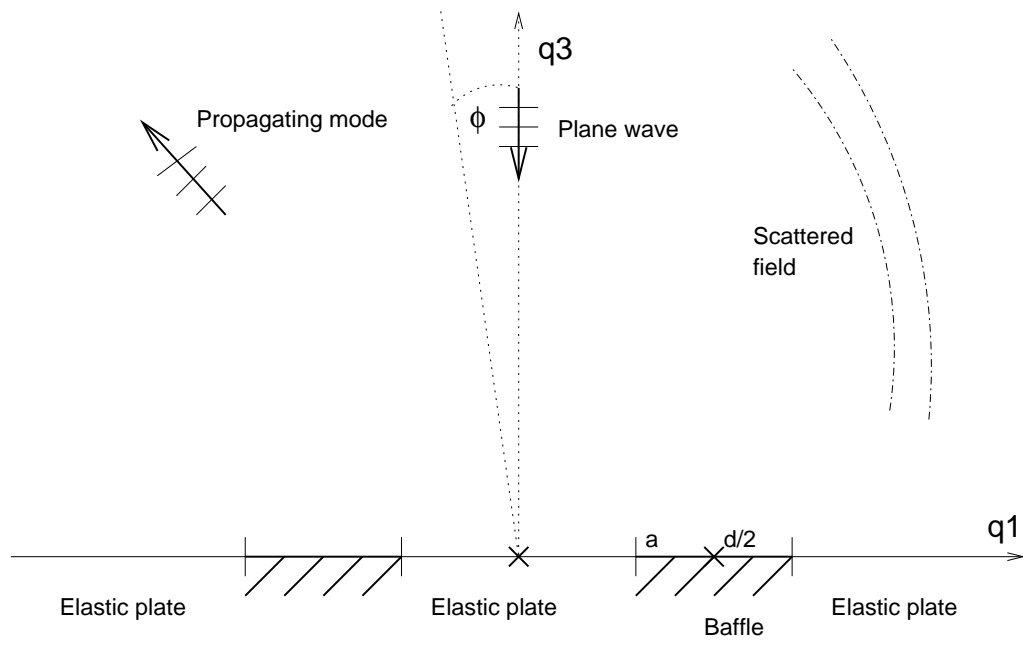


FIGURE 10.

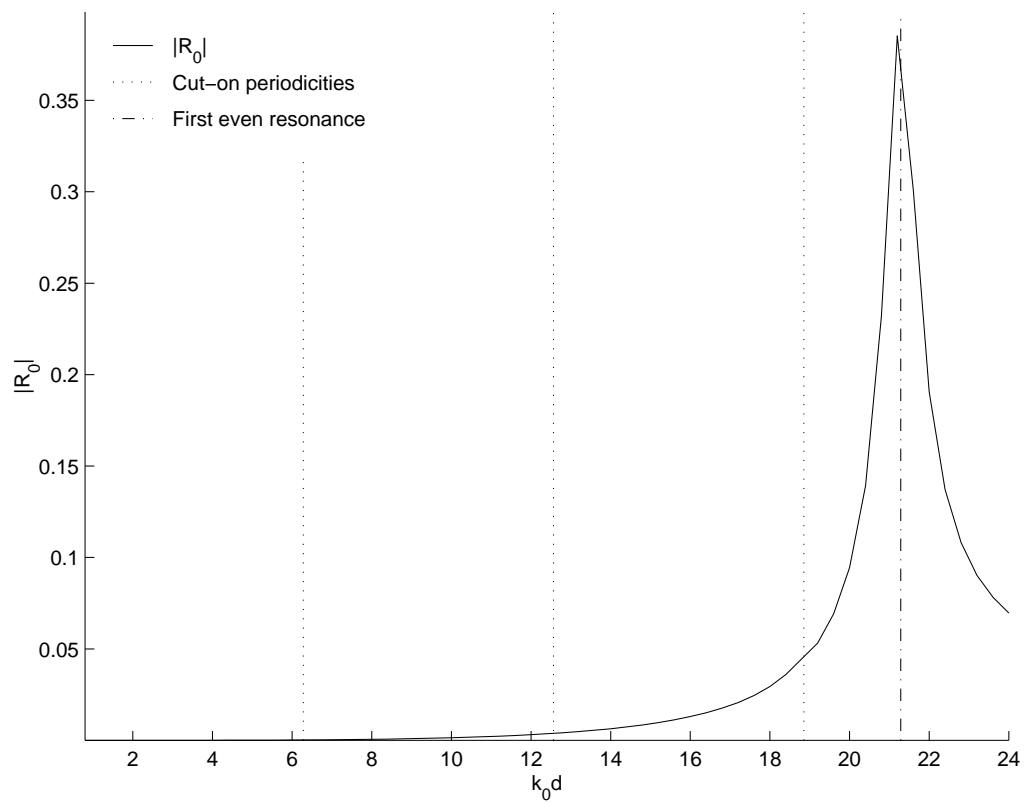


FIGURE 11.